Chemistry–A European Journal
Research Article
doi.org/10.1002/chem.202404233
Chemistry Europe
European Chemical Societies Publishing
www.chemeurj.org

Hot Paper

The Impact of Single Amino Acid Insertion on the Supramolecular Assembly Pathway of Aromatic Peptide Amphiphiles

Ayato Higuchi,[a] Arka Som,[c] Rie Wakabayashi,*[a] Masahiro Goto,*[a, b] Noriho Kamiya,*[a, b] and Pol Besenius*[c]

Understanding the mechanism of self-assembly driven by non-covalent interactions is crucial for designing supramolecular materials with desired properties. Here we investigate the self-assembly of aromatic peptide amphiphiles, Fmoc-L_2QG and Fmoc-L_3QG using a combination of spectroscopic, transmission electron and superresolution optical microscopy techniques. Our results show that Fmoc-L_2QG leads to concentration-dependent assembly, forming fibrous assemblies at low concentrations and supramolecular droplets via liquid-liquid phase separation (LLPS) at higher concentrations. Mechanical activation using for example ultrasonication triggered the transition from metastable droplets to fibre morphologies of Fmoc-L_2QG. In contrast, Fmoc-L_3QG followed both on-pathway and off-pathway routes, resulting in the formation of fibrous morphologies regardless of concentration. Seeding experiments revealed that homo-seeds of the same peptide sequence accelerated the on-pathway process, while hetero-seeds of a mismatched peptide sequences accelerated the off-pathway process, highlighting the competing nature of the complex assembly profile. These findings demonstrate the significant impact of single amino acid insertion on the supramolecular assembly process of oligopeptide monomers, and highlight the potential for controlling the structure and dynamics of peptide materials. Pathway engineering of oligopeptide building blocks and multidomain supramolecular monomers will open new avenues in tailor-made and customizable supramolecular biomaterials.

Introduction

Self-assembly driven by non-covalent interactions is ubiquitous in both natural and synthetic systems, drawing significant research interest.[1] Mechanistically the self-assembly process is composed of three steps: nucleation, fragmentation, and elongation, each playing a crucial role in the formation of supramolecular polymers and materials.[2] Self-assembly processes involve multiple competing pathways that are both kinetically and thermodynamically stable, leading to the formation of supramolecular materials with different structures and functions depending on the pathway.[1b,3] Classical nucleation theory generally fails to explain all aspects of how complex and ordered structures arise from simple building blocks and fails to adequately address polymorphism and the involved phase transitions.[4] Recent studies have for example highlighted the role of liquid-liquid phase separation (LLPS) in the assembly mechanism and its impact as intermediate process which promotes nucleation and subsequent growth.[4b,5] Desolvation has been reported to play a major role in the formation of droplets generated by LLPS and hence can account for the emergence of complex structures in peptide assembly, whereas directional intermolecular interactions, such as hydrogen bonding and π-π stacking interactions, are crucial for forming ordered morphologies from these droplets.[6] Therefore, a detailed understanding of the kinetically and thermodynamically controlled pathways of supramolecular polymerization and peptide assembly is essential to obtain materials with desirable structural, dynamic and functional properties.[3,7] To this end mechanistic investigations of supramolecular assembly and kinetic studies are critical.[8] In cases where muiltiple competing interactions and pathways are involved, supramolecular assembly routes are generally divided into on- and off-pathways. In the first case and on-pathway, monomeric building blocks are consumed through nucleation and elongation en route to the assembled superstructure. A mechanism involving an intermediate step that promotes nucleation and subsequent growth via LLPS is a special case of on-pathway assembly. In contrast, in the off-pathway route monomers are consumed at the expense of the thermodynamic or target product formation, leading to a different supramolecular polymorph. On- and off-

[a] A. Higuchi, R. Wakabayashi, M. Goto, N. Kamiya
Department of Applied Chemistry, Graduate School of Engineering, Kyushu University, 744 Motooka, Nishi-ku, Fukuoka 819–0395, Japan
E-mail: wakabayashi.rie.122@m.kyushu-u.ac.jp
m-goto@mail.cstm.kyushu-u.ac.jp
kamiya.noriho.367@m.kyushu-u.ac.jp
[b] M. Goto, N. Kamiya
Center for Future Chemistry, Kyushu University, Fukuoka 819–0395, Japan
[c] A. Som, P. Besenius
Department of Chemistry, Johannes Gutenberg-University Mainz, Duesbergweg 10– 14, D-55128 Mainz, Germany
E-mail: besenius@uni-mainz.de

Supporting information for this article is available on the WWW under https://doi.org/10.1002/chem.202404233

pathway routes often compete and the preferred pathway is determined by the energy barriers that are involved,[3,7] while nucleation events in competing pathways can be manipulated externally using pH,[9] photochemistry,[10] redox chemistry[11] and intramolecular interactions.[12]

Peptide Amphiphiles (PAs) have been established as versatile building blocks for supramolecular material assembly in aqueous media.[13] In particular, PAs with aromatic moieties are known to form a variety of structures driven by π-π stacking between aromatic components and β-sheet-like hydrogen bonding,[3g,14] and it has been reported that small differences in the amino acid sequence can significantly affect the morphology of the structures.[15] We have previously reported on a novel short aromatic peptide amphiphile, 9-fluorenylmethoxycarbonyl-(Leu)$_n$-Gln-Gly (Fmoc-L$_n$QG, n = 2 or 3). Fmoc-L$_n$QG forms assemblies through cooperative π-π stacking interactions between Fmoc groups and hydrogen bonding in the peptide backbone. Our initial investigations suggested that Fmoc-L$_2$QG primarily relies on π-π stacking, while Fmoc-L$_3$QG primarily relies on hydrogen bonds as the main driving force for supramolecular assembly.[16] However, it remains completely unclear whether the differences in the previously observed molecular packing and structure formation are due to the supramolecular encoded oligopeptide sequence itself or are a result of the sample preparation and thus assembly protocol. In this study, we therefore aimed to elucidate the assembly pathways of both building blcoks Fmoc-L$_2$QG and Fmoc-L$_3$QG (Figure 1a) through detailed spectroscopic and microscopic investigations. Our experiments using Fmoc-L$_2$QG exhibit two distinct assembly mechanisms in low and high-concentration regimes (Figure 1b), where the high-concentration regime reveals an intermediate metastable state which proceeds via Liquid-Liquid Phase Separation (LLPS). In contrast, insertion of one leucine amino acid in Fmoc-L$_3$QG is found to follow a self-assembly mechanism into fibres involving both on-pathway and off-pathway routes (Figure 1b).

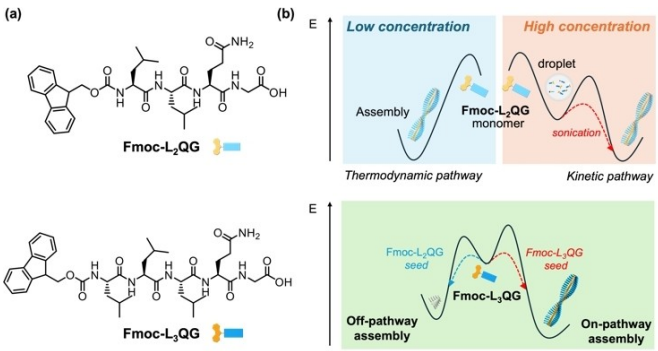

Figure 1. (a) Chemical structures of Fmoc-L$_2$QG (above), Fmoc-L$_3$QG (below). (b) Energy landscapes for the assembly processes of Fmoc-L$_2$QG (above), Fmoc-L$_3$QG (below).

Results and Discussion

Kinetic Measurements of Fmoc-L$_n$QG (n = 2, 3) Assembly

Fmoc-L$_n$QG (n = 2, 3) was synthesized using Fmoc peptide solid-phase synthesis method according to previous studies (Figure S1).[16] To gain insights into the assembly mechanisms of these peptide amphiphiles (PAs), concentration-dependent self-assembly kinetics were investigated by circular dichroism (CD) spectroscopy.[17] The assembly half-time, t_{50}, is defined as the time point at which the formation of assemblies reaches half-completion. The slope (γ) and curvature of the double-logarithmic plot of PA concentration and t_{50} are crucial indicators for understanding the mechanism of supramolecular peptide assembly. These parameters provide insights into the detailed mechanisms and dominant pathways of the supramolecular assembly process.[2b,18] Specifically, a scaling exponent (γ) around −0.5 indicates a pathway dominated by nucleating-elongation-fragmentation processes, while a more negative slope ($\gamma < -0.5$) suggests that secondary nucleation is dominant. A change in slope and negative curvature indicates that there is competition between parallel processes, while a positive curvature is characteristic of serial pathways. On the other hand, a positive scaling exponent ($\gamma > 0$) is a rather rare phenomenon and implies that depletion effects occur throughout the self-assembly process due to the presence of off-pathway mechanisms.[9,19] In this case nuclei formed via the off-pathway compete for monomers with nuclei in the on-pathway during the supramolecular assembly process, and the depletion of monomeric species buffers the progression for on-pathway assembly formation.

The assembly kinetics and experiments for both building blocks Fmoc-L$_n$QG (n = 2, 3) were performed in a homogenous mixture of two solvents, hexafluoro-2-propanol (HFIP), a hydrogen bond donor, and phosphate-buffered saline (PBS) at pH 7.4. In aqueous buffer supramolecular assembly into ordered peptide fibres was previously reported.[16] However, for kinetic experiments, the time-scale of aggregation in buffered H_2O was too fast and did not allow us to perform concentration dependent kinetic investigations. We therefore prepared molecularly dissolved concentrated solutions Fmoc-L$_n$QG in HFIP. The lack of characteristic CD signatures indicated the presence of monomeric, non-aggregated, aromatic peptide amphiphiles (Figure S2).

To follow the time-dependent aggregation kinetics, concentrated solutions of Fmoc-L$_n$QG (n = 2, 3) in HFIP were diluted into PBS in ratios of 49:1 to 8:1 PBS: HFIP (*V:V*) at 5 °C as shown in Figure 2a. The individual CD spectra were measured and the intensity of the characteristic CD bands plotted as a function of time in order to determine the concentration dependent t_{50} values according to formula (1) for each buildings block. The supramolecular assembly formation of Fmoc-L$_2$QG was too rapid to determine t_{50} under the condition of PBS: HFIP = 49:1 (Figure S3). In contrast, under the same conditions the assembly kinetics of Fmoc-L$_3$QG were slower compared to Fmoc-L$_2$QG, and we first investigated the assembly mechanism of Fmoc-L$_3$QG by calculating t_{50} at various concentrations

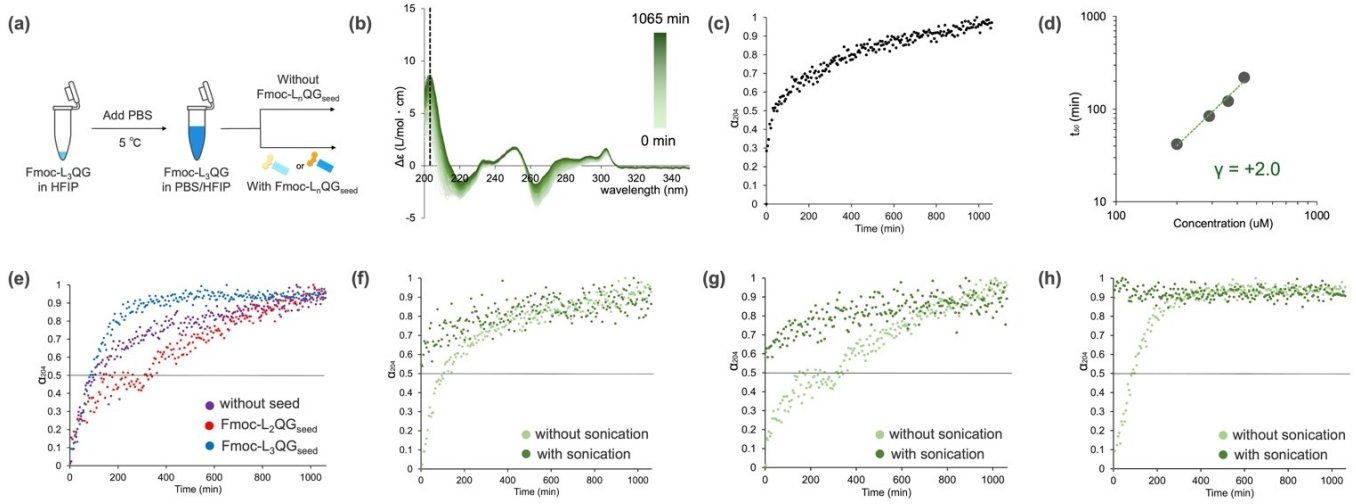

Figure 2. (a–d) Kinetics and (e–f) seeding measurement of Fmoc-L_3QG. (a) Experimental scheme of kinetics measurement (above) and seed experiments (below), (b) Time dependent CD spectra of Fmoc-L_3QG (200 μM) in PBS/HFIP (49:1) at 5 °C. (c) Degree of aggregation (α) for the kinetic experiments of Fmoc-L_3QG (200 μM) in PBS/HFIP. (d) Double logarithmic plot for the aggregation half times t_{50} of the assembly of Fmoc-L_3QG (200, 290, 360, 430 μM). (e) Degree of aggregation (α) of Fmoc-L_3QG (360 μM, purple), Fmoc-L_3QG (360 uM) added Fmoc-L_2QG$_{seed}$ (3.6 μM, red) or Fmoc-L_3QG$_{seed}$ (3.6 μM, blue) in PBS/HFIP (49:1). Degree of aggregation (α) of (f) Fmoc-L_3QG (360 μM), (g) Fmoc-L_3QG (360 μM) added Fmoc-L_2QG$_{seed}$ (3.6 μM), (h) Fmoc-L_3QG (360 μM) added Fmoc-L_3QG$_{seed}$ (3.6 μM) without/with ultrasonic irradiation.

(200 μM–430 μM) through CD spectroscopy experiments. A positive CD band at λ = 204 nm and a negative band at λ = 220 nm, indicative of β-sheet formation, increased in intensities over time (Figure 2b). These characteristic CD signatures were observed for all samples of Fmoc-L_3QG, regardless of the sample concentration (Figure S4). The normalized data and degree of aggregation (α) at each time point was calculated using formula (1) by monitoring the intensity of the CD band at λ = 204 nm (Figure 2c). The t_{50} values at various peptide concentrations was determined through curve fitting (Figure S5). Intriguingly, when plotting the concentration dependent t_{50} values in a double-logarithmic plot, a positive slope of γ = +2.0 was obtained for Fmoc-L_3QG (Figure 2d). This result suggests the presence of competing on-/off-pathways.[2b,3a,h,9]

To corroborate these results and gain further insights into the assembly process of Fmoc-L_3QG, the t_{50} was evaluated under conditions with added seeds. Seeding experiments, their impact on assembly kinetics are essential for a detailed understanding of supramolecular assembly mechanisms and pathways, as the presence of seeds directly controls nucleation and growth processes.[3c,7a,20] Fmoc-L_2QG$_{seed}$ was used as hetero-seed with a mismatched peptide sequence which lacks one leucine amino acid, and Fmoc-L_3QG$_{seed}$ was used as homo-seed. The solutions of seeds were prepared by equilibrating a solution of aggregated Fmoc-L_nQG at low monomer concentration (36 μM) in PBS/HFIP (49:1). The seeding experiments were performed by adding Fmoc-L_nQG$_{seed}$ to Fmoc-L_3QG using the same sample preparation method as described for the non-seeded experiments, using a monomer to seed ratio [Fmoc-L_3QG]: [Fmoc-L_nQG$_{seed}$] = 100:1. The degree of aggregation (α) at each time point was again calculated using formula (1) by monitoring the intensity of the CD band at λ = 204 nm (Figure S6). At a Fmoc-L_3QG monomer concentration of 360 μM, the t_{50} value of 122 min in absence of seeds decreased to t_{50} = 88 min in presence of added homo-seed Fmoc-L_3QG$_{seed}$ (Figure 2e). Furthermore, that t_{50} was decreased by ultrasonic irradiation regardless of whether seeds were added or not (Figure 2f–h). These results indicate that the presence of Fmoc-L_3QG$_{seeds}$ is essential to nucleate formation of Fmoc-L_3QG assemblies. Surprisingly, the addition of hetero-seeds (Fmoc-L_2QG$_{seeds}$) to a solution Fmoc-L_3QG of extended t_{50} to 253 min (Figure 2e). We hypothesise that seeds based on mismatched peptide sequence are unable to catalyse the on-pathway process and instead favour off-pathway products via unspecific binding and depletion of free monomers.

For Fmoc-L_2QG, the supramolecular assembly kinetics were slowed down by adding HFIP to buffered water, yet the relative volume fraction of HFIP had to be increased to a ratio PBS: HFIP = 8:1 (*V:V*) in order to investigate concentration dependent t_{50} on a feasible time-scale using CD spectroscopy. At various concentrations a positive CD band at λ = 218 nm and a broad positive band between λ = 250–270 nm was attributed to hydrogen bonded peptide domains and π-π stacking interactions of Fmoc groups (Figure 3a and S7). The normalized data and degree of aggregation (α) at each time point of the kinetics investigations was calculated using the intensity of the CD band at λ = 218 nm (Figure 3b and S8). The t_{50} at various peptide concentrations was determined through curve fitting and in the double-logarithmic plot a change in slope (negative curvature) from low to high Fmoc-L_2QG concentrations could clearly be observed (Figure 3c). In the lower concentration regime (< 450 μM) a scaling exponent was found to be γ = −0.4. This suggests a supramolecular assembly mechanism which is dominated by nucleation-elongation-fragmentation process.[2b,8e,18b] In contrast, in the higher concentration regime (> 450 μM) the scaling exponent decreases significantly to γ =

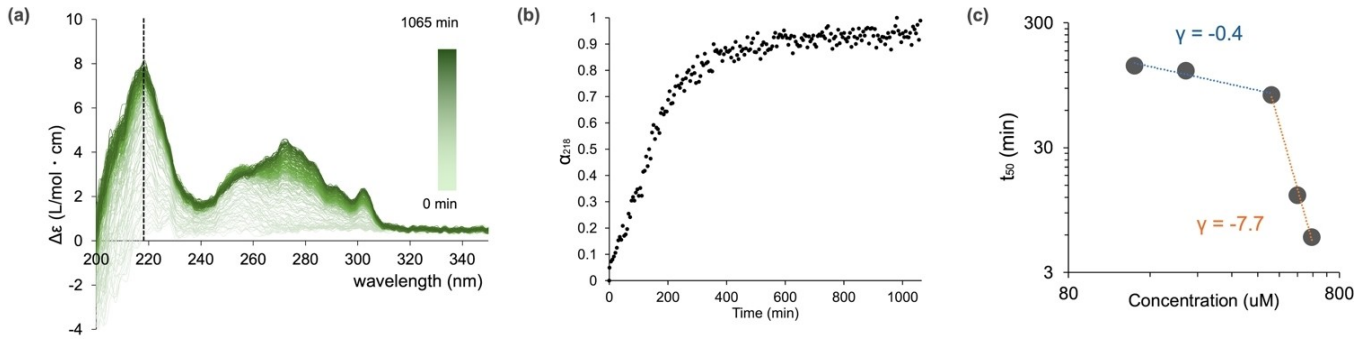

Figure 3. (a) Time over CD spectra (light green : 0 min, dark green: 1065 min) of Fmoc-L_2QG (150 μM) in PBS/HFIP (8:1) at 5 °C. Inset: The scheme of CD experiment protocol. (b) Degree of aggregation (α) for the kinetic measurement of Fmoc-L_2QG (150 μM). (c) Double logarithmic plot of the half times t_{50} of the assembly of Fmoc-L_2QG (150, 220, 450, 560, 630 μM).

−7.7, which suggests a change in mechanism and likely heterogeneous nucleation plays a dominant under these conditions. These findings motivated us to perform microscopic investigations to resolve the morphology of the aromatic peptide amphiphiles and potential structural transitions in the relevant concentration regimes for Fmoc-L_2QG and Fmoc-L_3QG, since structure, dynamics and function are intimately related and an integral part of supramolecular materials design and applications.[3,7]

Morphological Transitions of Fmoc-L_nQG (n = 2, 3)

The morphology of Fmoc-L_nQG (n = 2, 3) assemblies in PBS/HFIP was investigated using high-resolution fluorescence microscopy, specifically structured illumination microscopy (SIM). Monomeric PA stock solutions were prepared by dissolving each PA in HFIP. A library of different concentrations was prepared by diluting the PA stock solution from HFIP into PBS on an ice bath. The PAs were then allowed to assemble and equilibrate by incubation at 5 °C. Imaging was performed using Thioflavin T (ThT) as a dye to visualize the supramolecular structures. Fmoc-L_2QG formed fibrous assemblies at low monomer concentrations (400 μM), but surprisingly supramolecular droplets were observed at high monomer concentrations (550 μM) (Figure 4a, b). These were confirmed even when varying the concentration of ThT, indicating that the formation of supramolecular droplets was not due to ThT itself (Figure S9). To confirm the liquid properties of the formed droplets, fluorescence recovery after photobleaching (FRAP) experiments were conducted within the spherical droplets (Figure S12). The rapid recovery of fluorescence intensity to about 60 % after 30 s is a strong indication of the fluid-like nature of the supramolecular droplets. To gain further insight into the assembly process, TEM experiments were performed. For Fmoc-L_2QG at lower concentrations (360 μM), fibrous assemblies (width: 10 nm) were found after the addition of PBS (Figure 4d), while at higher concentrations (550 μM) some larger droplets (diameter: 3–4 μm) could be observed (Figure 4e), an observation which was consistent with results from SIM experiments.

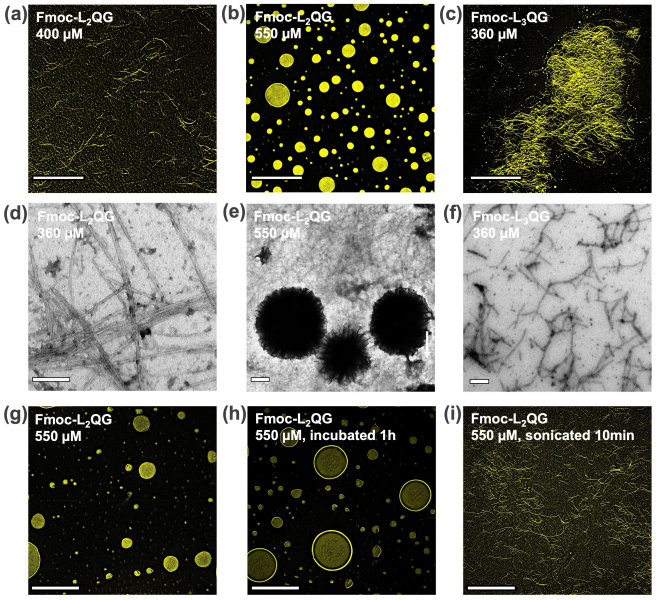

Figure 4. Microscopic characterization of Fmoc-L_nQG (n = 2, 3) assembly: SIM images of Fmoc-L_2QG assembly at (a) 400 μM, (b) 550 μM, and (c) Fmoc-L_3QG assembly at 360 μM containing ThT (150 μM); scale bars: 20 μm. TEM images of Fmoc-L_2QG assembly at (d) 360 μM, (e) 550 μM and Fmoc-L_3QG assembly at (e) 360 μM; scale bars: (d, f) 200 nm, (e) 1 μm. SIM images of Fmoc-L_2QG assembly at (g) 550 μM, (h) after incubation for 1 h and (i) after sonication for 10 min; scale bars: 20 μm.

For Fmoc-L_3QG, only fibrous assemblies (width: 17 nm) were observed (Figure 4f).

We were further intrigued to investigate the stability of the droplets using SIM. By diluting the concentrated droplet solution of Fmoc-L_2QG (550 μM) to a lower concentration (400 μM) the structural transition from supramolecular droplets to fibrous assemblies was observed instantly (Figure S10). This observation suggests that the transition into a demixed state of a peptide-depleted dilute phase and a peptide-enriched condensed phase is concentration dependent and produces a metastable state with transient stability. In addition, ultrasound irradiation at a constant concentration induced the structural change from supramolecular droplets to fibrous assemblies (Figure 4g–i), confirming the metastable nature of the phase separated state.

By combining the spectroscopy and microscopy experiments, we are thereby able to eludicate a complex energy landscape. The concentration dependent supramolecular assembly kinetics of Fmoc-L_2QG ($\gamma = -0.4$) are indicative of a nucleation-elongation-fragmentation mechanism at monomer concentrations <450 μM. At higher concentrations (>450 μM) CD spectroscopy and superresolution microscopy clearly suggest that the supramolecular polymerization produces β-sheet ordered nanofibers via a non-classical multi-step process: SIM and TEM provide evidence for liquid-liquid phase separation during supramolecular assembly into peptide-rich liquid droplets (Figure 5a). These metastable droplets most likely arise from desolvation of aggregating peptides and heterogenous nucleation events dominate the supramolecular assembly kinetics. This is supported by the unusually low scaling exponent ($\gamma = -7.7$) in the CD monitored concentration dependent supramolecular assembly kinetics in the regime >450 μM. In contrast, the corresponding experiments for Fmoc-L_3QG show no sign of LLPS or droplet formation, and give rise to a positive scaling exponent ($\gamma = 2.0$) which is a hallmark of pathway complexity and competing on-/off-pathways (Figure 5b).

Conclusions

This study elucidates the intricate self-assembly mechanisms of the aromatic peptide amphiphiles Fmoc-L_2QG and Fmoc-L_3QG, emphasizing the significant impact of inserting a single amino acid into the oligopeptide sequence of Fmoc-L_2QG. Detailed kinetic and morphological analyses revealed that Fmoc-L_2QG exhibits distinct self-assembly behavior at varying concentrations, with high concentrations leading to intermediate droplet formation via LLPS, and low concentrations resulting in fibrous structures (Figure 5a). The kinetic experiments indicate that at low concentrations supramolecular assembly into fibres is governed by nucleation-elongation-fragmentation, while at at high concentrations the assembly process is dominated by heterogeneous nucleation. In contrast, Fmoc-L_3QG follows both on-pathway and off-pathway assembly routes (Figure 5b). Seeding experiments demonstrated that homo-seeds of Fmoc-L_3QG accelerate the on-pathway process, while hetero-seeds of a mismatched sequence (Fmoc-L_2QG) accelerate the off-pathway process, highlighting the competing nature of the complex assembly profile. These findings provide insights into the role of specific amino acid sequences in dictating the self-assembly pathways and resulting morphologies of peptide amphiphiles. Manipulating the energy landscape of supramolecular peptide materials by controlling the assembly protocol of the building block will open new opportunities for tailor-made and customizable supramolecular biomaterials.

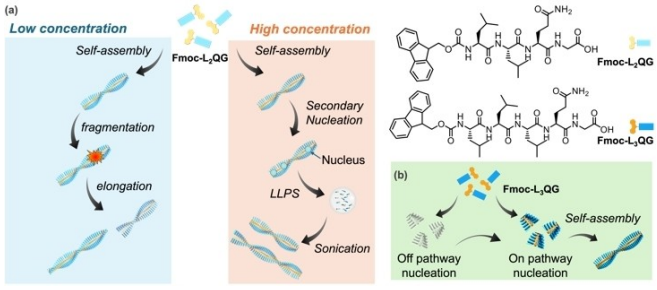

Figure 5. Proposed mechanism for (a) Fmoc-L_2QG and (b) Fmoc-L_3QG supramolecular assembly formation.

Experimental Section

General

The amino acid reagents and resin for the synthesis of PAs, Fmoc-Gly-Alko-resin, Fmoc-Leu-OH, Fmoc-Gln(Trt)-OH, O-(1H-benzotriazol-1-yl)-N,N,N′,N′-tetramethyluronium hexafluorophosphate (HBTU), 1-hydroxy-1-H-benzotriazole hydrate (HOBt), N,N-diisopropylethylamine (DIEA), piperidine, trifluoroacetic acid (TFA), and triisopropylsilane (TIS) were purchased from Watanabe Chemical Industries (Hiroshima, Japan). Reagents for the Kaiser test were purchased from Kokusan Chemical (Tokyo, Japan). Methanol, dichloromethane, diethyl ether, acetonitrile (ACN), sodium hydrogenphosphate dodecahydrate, and trizma base were obtained from Wako Pure Chemical Industries (Osaka, Japan). *N*,*N*-dimethylformamide (DMF), dimethyl sulfoxide (DMSO), triethylamine (TEA), acetic acid (AcOH), Phospate Buffered Saline (PBS), Thioflavin T (ThT) were obtained from Sigma Aldrich (St. Louis, MO, USA). Trifluoroethanol (TFE) was obtained from Tokyo Chemical industry (Tokyo, Japan). 1,1,1,3,3,3-Hexafluorpropan-2-ol (HFIP) was obtained from Carbolution (Kaiserstraße, Germany)

Material Synthesis[16]

Fmoc-L_nQG (n = 2, 3) was synthesized via standard 9-fluorenylmethoxycarbonyl (Fmoc) solid-phase peptide synthesis. Fmoc-Gly-Alko Resin was immersed in dichloromethane for 30 min. The protective Fmoc group was removed using 20% piperidine in DMF. The deprotection was confirmed by Kaiser tests. Coupling reactions of each amino acid were conducted by adding a mixture of coupling reagents (Fmoc-amino acid:HBTU:HOBt:DIEA = 3:3:3:6 mol equivalent to reactive sites on resin) in DMF to the resin and shaken for 1 h. After coupling reactions, the protective Fmoc group was removed by 20% piperidine in DMF except for the last amino acid. The aromatic peptides were cleaved from the resin using a mixture of 95% TFA, 2.5% TIS, and 2.5% water for 1.5 h. After removing the solvents under reduced pressure, the peptides were precipitated and washed with cold diethyl ether. The crude peptide solids were collected, and dissolved in the mixture of DMSO, TFE, and a 0.1% aqueous solution of TEA/AcOH (11:2 (*V*/*V*)) with a 2:2:6 (*V*/*V*/*V*) ratio, and purified by reverse-phase high-pressure liquid chromatography (HPLC) on Inertsil ODS-3 column (GL Science, Tokyo, Japan) using a gradient of water and acetonitrile both containing 0.1% TEA/AcOH. The fractions with each PA were collected, lyophilized, and stored at −20 °C until use. The purified peptides were analyzed by HPLC (Inertsil ODS-3 column, GL Science, Tokyo, Japan) and MALDI TOF MS (Autoflex-III, Bruker, Billerica, MA, USA) using α-cyano-4-hydroxycinnamic acid (CHCA, Sigma-Aldrich (St. Louis, MO, USA)) as the matrix.

Fmoc-L_nQG (n = 2, 3) Sample Preparation

Monomeric PA stock solutions were prepared by dissolving each PA in HFIP (20 mM), a hydrogen bond donor solvent. Measurement samples of various concentrations were prepared by diluting the

PA stock solution in HFIP with PBS in an ice bath. Fmoc-L_2QG was diluted to a ratio of PBS: HFIP = 8:1 (*V/V*), and Fmoc-L_3QG to a ratio of PBS: HFIP = 49:1 (*V/V*).

Kinetic CD Spectroscopy Experiments[17]

Immediately after preparing the sample solution, the solution was added to a cell with an optical path length of 1 mm, and the CD spectra (JASCO, J-815) were measured over time (time interval: 5 min, scan speed: 50 nm/min, range: 190–350 nm, sensitivity: standard, temperature: 5 °C). The degree of association α at each time point was calculated using Equation (1), and a plot was created. Curve fitting was performed on the obtained plot using ImageJ, and the time to reach $\alpha = 0.5$ (half time, t_{50}) was calculated from the approximate curve.

Seeding Experiments

Fmoc-L_nQG_{seed} was prepared by creating a low monomer concentration (36 μM) solution that does not form assemblies, following the same method as for the CD measurement samples (PBS: HFIP = 49:1 (*V/V*)). After diluting the Fmoc-L_3QG solution dissolved in HFIP with PBS, the prepared Fmoc-LnQG_{seed} solution was added to prepare the measurement solution ([Fmoc-L_3QG]: [Fmoc-L_nQG_{seed}] - = 360 μM : 3.6 μM (100:1 (mol : mol)). Immediately after preparing the measurement solution, the half-time (t_{50}) was calculated following the same procedure as in the kinetic CD spectroscopy experiments.

Super-Resolution Fluorescence Microscope Images of Fmoc-L_nQG (n = 2, 3) Assembly

ThT solution at a final concentration of 150 μM was added to the prepared samples. The samples with ThT (150 μL) were transferred into glass-bottom dishes. The super-resolution fluorescence microscope images were taken using structured illumination microscopy (SIM) mode on Elyra 7 using a lattice spot pattern. 13 phases were acquired and image reconstruction was performed in the Zeiss (Oberkochen, Germany) Zen Black software. The excitation used for the study is 488 nm.

Transmission Electron Microscopy (TEM)

Fmoc-L_2QG (360, 550 uM) and Fmoc-L_3QG (360 uM) were prepared in PBS/HFIP the same way as for kinetic CD spectroscopy measurements. 2 μL of each sample were drop-cast onto a hydrophilized STEM grid with an elastic carbon film (Okenshoji, Tokyo, Japan). After 2 minutes of incubation, the excess solution was removed and washed with 2.5 μL of MilliQ. It was stained with 2% uranyl solution for 2 minutes. The transmission electron microscopy (TEM) images were taken by JEM-2010 (JEOL, Tokyo, Japan) with an accelerating voltage of 120 kV.

Acknowledgements

We acknowledge financial support by the Gutenberg Research College, the Deutsche Forschungsgemeinschaft (DFG) through project number 497845157 and the Research Training Group RTG 2516 (project number 405552959) [P.B.], the European Research Council (ERC) under the European Union's Horizon 2020 research and innovation programme (ERC CoG SUPRA-VACC - 819856) [A.S., P.B.], and the DAAD (PPP-DST project 57711219) [P.B.]. This work was supported by JSPS KAKENHI Grant Numbers JP22H01884 [R.W. and N.K.] and JP22KJ2482 [A.H.], JSPS Bilateral Program Number JPJSBP120243507 [R.W., N.K. and M.G.], JSPS Overseas Challenge Program for Young Researchers (No. 202380251) [A.H.], and the Uehara Memorial Foundation [R.W.]. Open Access funding enabled and organized by Projekt DEAL.

Conflict of Interests

The authors declare no conflict of interest.

Data Availability Statement

The data that support the findings of this study are available from the corresponding author upon request.

Keywords: Aromatic peptide amphiphile · Supramolecular polymerisation · Pathway complexity · Competing pathways · Liquid-liquid phase separation

[1] a) T. Aida, E. W. Meijer, S. I. Stupp, *Science* **2012**, *335*, 813–817; b) E. Mattia, S. Otto, *Nat. Nanotechnol.* **2015**, *10*, 111–119; c) K. Tao, P. Makam, R. Aizen, E. Gazit, *Science* **2017**, *358*, eaam9756.

[2] a) A. Sorrenti, J. Leira-Iglesias, A. J. Markvoort, T. F. A. Greef, T. M. Hermans, *Chem. Soc. Rev.* **2017**, *46*, 5476–5490; b) G. Meisl, L. Rajah, S. A. I. Cohen, M. Pfammatter, A. Šarić, E. Hellstrand, A. K. Buell, A. Aguzzi, S. Linse, M. Vendruscolo, C. M. Dobson, T. P. J. Knowles, *Chem. Sci.* **2017**, *8*, 7087–7097; c) S. Linse, *Pure Appl. Chem.* **2019**, *91*, 211–229.

[3] a) P. A. Korevaar, S. J. George, A. J. Markvoort, M. M. J. Smulders, P. A. J. Hilbers, A. P. H. J. Schenning, T. F. A. Greef, E. W. Meijer, *Nature* **2012**, *481*, 492–496; b) S. Ogi, K. Sugiyasu, S. Manna, S. Samitsu, M. Takeuchi, *Nat. Chem.* **2014**, *6*, 188–195; c) S. Ogi, T. Fukui, M. L. Jue, M. Takeuchi, K. Sugiyasu, *Angew. Chem. Int. Ed.* **2014**, *53*, 14363–14367; d) P. A. Korevaar, T. F. A. Greef, E. W. Meijer, *Chem. Mater.* **2014**, *26*, 576–586; e) F. Tantakitti, J. Boekhoven, X. Wang, R. V. Kazantsev, T. Yu, J. Li, E. Zhuang, R. Zandi, J. H. Ortony, C. J. Newcomb, L. C. Palmer, G. S. Shekhawat, M. O. La Cruz, G. C. Schatz, S. I. Stupp, *Nat. Mater.* **2016**, *15*, 469–476; f) S. Ogi, C. Grzeszkiewicz, F. Würthner, *Chem. Sci.* **2018**, *9*, 2768–2773; g) W. Ji, S. Zhang, S. Yukawa, S. Onomura, T. Sasaki, K. i. Miyazawa, Y. Zhang, *Angew. Chem. Int. Ed.* **2018**, *57*, 3636–3640; h) J. Matern, Y. Dorca, L. Sánchez, G. Fernández, *Angew. Chem. Int. Ed.* **2019**, *58*, 16730–16740; i) J. Matern, K. K. Kartha, L. Sánchez, G. Fernández, *Chem. Sci.* **2020**, *11*, 6780–6788; j) M. Wehner, F. Würthner, *Nat. Rev. Chem.* **2020**, *4*, 38–53; k) F. Wang, R. Liao, F. Wang, *Angew. Chem. Int. Ed.* **2023**, *62*, e202305827.

[4] a) L. Houben, H. Weissman, S. G. Wolf, B. Rybtchinski, *Nature* **2020**, *579*, 540–543; b) C. Yuan, Q. Li, R. Xing, J. Li, X. Yan, *Chem* **2023**, *9*, 2425–2445; c) J. S. Du, Y. Bae, J. J. De Yoreo, *Nat. Rev. Mater.* **2024**, *9*, 229–248.

[5] a) L. Su, J. Mosquera, M. F. J. Mabesoone, S. M. C. Schoenmakers, C. Muller, M. E. J. Vleugels, S. Dhiman, S. Wijker, A. R. A. Palmans, E. W. Meijer, *Science* **2022**, *377*, 213–218; b) S. Patra, S. Chandrabhas, S. Dhiman, S. J. George, *J. Am. Chem. Soc.* **2024**, *146*, 12577–12586; c) H. Duijs, M. Kumar, S. Dhiman, L. Su, *J. Am. Chem. Soc.* **2024**, *146*, 29759–29766.

[6] a) C. Yuan, A. Levin, W. Chen, R. Xing, Q. Zou, T. W. Herling, P. K. Challa, T. P. J. Knowles, X. Yan, *Angew. Chem. Int. Ed.* **2019**, *58*, 18116–18123; b) Y. Lin, Y. Fichou, A. P. Longhini, L. C. Llanes, P. Yin, G. C. Bazan, K. S. Kosik, S. Han, *J. Mol. Biol.* **2021**, *433*, 166731; c) M. Abbas, W. P. Lipiński, J. Wang, E. Spruijt, *Chem. Soc. Rev.* **2021**, *50*, 3690–3705; d) F. Späth, C. Donau, A. M. Bergmann, M. Kränzlein, C. V. Synatschke, B. Rieger, J. Boekhoven, *J. Am. Chem. Soc.* **2021**, *143*, 4782–4789; e) A. Jain, S. Kassem, R. S. Fisher, B. Wang, T.-D. Li, T. Wang, Y. He, S. Elbaum-

Garfinkle, R. V. Ulijn, *J. Am. Chem. Soc.* **2022**, *144*, 15002–15007; f) R. Kubota, T. Hiroi, Y. Ikuta, Y. Liu, I. Hamachi, *J. Am. Chem. Soc.* **2023**, *145*, 18316–18328; g) P. Zhou, R. Xing, Q. Li, J. Li, C. Yuan, X. Yan, *Matter* **2023**, *6*, 1945–1963; h) D. Sementa, D. Dave, R. S. Fisher, T. Wang, S. Elbaum-Garfinkle, R. V. Ulijn, *Angew. Chem. Int. Ed.* **2023**, *62*, e202311479; i) A. Leppert, G. Chen, D. Lama, C. Sahin, V. Railaite, O. Shilkova, T. Arndt, E. G. Marklund, D. P. Lane, A. Rising, M. Landreh, *Nano Lett.* **2023**, *23*, 5836–5841; j) C. Yuan, R. Xing, J. Cui, W. Fan, J. Li, X. Yan, *CCS Chem.* **2024**, *6*, 255–265; k) S. Cao, T. Ivanov, J. Heuer, C. T. J. Ferguson, K. Landfester, L. Caire da Silva, *Nat. Commun.* **2024**, *15*, 39; l) R. Chang, C. Yuan, P. Zhou, R. Xing, X. Yan, *Acc. Chem. Res.* **2024**, *57*, 289–301.

[7] a) T. Fukui, S. Kawai, S. Fujinuma, Y. Matsushita, T. Yasuda, T. Sakurai, S. Seki, M. Takeuchi, K. Sugiyasu, *Nat. Chem.* **2017**, *9*, 493–499; b) W. Wagner, M. Wehner, V. Stepanenko, F. Würthner, *CCS Chem.* **2019**, *1*, 598–613; c) P. K. Hashim, J. Bergueiro, E. W. Meijer, T. Aida, *Prog. Polym. Sci.* **2020**, *105*, 101250; d) A. J. Dear, G. Meisl, A. Šarić, T. C. T. Michaels, M. Kjaergaard, S. Linse, T. P. J. Knowles, *Chem. Sci.* **2020**, *11*, 6236–6247; e) M. Muschol, W. Hoyer, *Front. Mol. Biosci.* **2023**, *10*, 1120416; f) R. M. Veedu, Z. Fernández, N. Bäumer, A. Albers, G. Fernández, *Chem. Sci.* **2024**, *15*, 10745–10752.

[8] a) A. Lohr, M. Lysetska, F. Würthner, *Angew. Chem. Int. Ed.* **2005**, *44*, 5071–5074; b) A. Ajayaghosh, R. Varghese, V. K. Praveen, S. Mahesh, *Angew. Chem. Int. Ed.* **2006**, *45*, 3261–3264; c) P. A. Korevaar, C. J. Newcomb, E. W. Meijer, S. I. Stupp, *J. Am. Chem. Soc.* **2014**, *136*, 8540–8543; d) P. Besenius, *J. Polym. Sci., Part A: Polym. Chem.* **2017**, *55*, 34–78; e) D. Spitzer, V. Marichez, G. J. M. Formon, P. Besenius, T. M. Hermans, *Angew. Chem. Int. Ed.* **2018**, *57*, 11349–11353.

[9] K. L. Zapadka, F. J. Becher, S. Uddin, P. G. Varley, S. Bishop, A. L. Gomes dos Santos, S. E. Jackson, *J. Am. Chem. Soc.* **2016**, *138*, 16259–16265.

[10] D. Gupta, A. Bhatt, V. Gupta, C. Miglani, J. P. Joseph, J. Ralhan, D. Mandal, M. E. Ali, A. Pal, *Chem. Mater.* **2022**, *34*, 4456–4470.

[11] D. Gupta, V. Gupta, D. Nath, C. Miglani, D. Mandal, A. Pal, *ACS Appl. Mater. Interfaces* **2023**, *15*, 25110–25121.

[12] a) J. Kang, D. Miyajima, T. Mori, Y. Inoue, Y. Itoh, T. Aida, *Science* **2015**, *347*, 646–651; b) S. Ogi, A. Takamatsu, K. Matsumoto, S. Hasegawa, S. Yamaguchi, *Angew. Chem. Int. Ed.* **2023**, *62*, e202306428.

[13] a) J. B. Matson, S. I. Stupp, *Chem. Commun.* **2012**, *48*, 26–33; b) S. S. Lee, T. Fyrner, F. Chen, Z. Álvarez, E. Sleep, D. S. Chun, J. A. Weiner, R. W. Cook, R. D. Freshman, M. S. Schallmo, K. M. Katchko, A. D. Schneider, J. T. Smith, C. Yun, G. Singh, S. Z. Hashmi, M. T. McClendon, Z. Yu, S. R. Stock, W. K. Hsu, E. L. Hsu, S. I. Stupp, *Nat Nano* **2017**, *12*, 821–829; c) M. P. Hendricks, K. Sato, L. C. Palmer, S. I. Stupp, *Acc. Chem. Res.* **2017**, *50*, 2440–2448.

[14] a) S. Fleming, R. V. Ulijn, *Chem. Soc. Rev.* **2014**, *43*, 8150–8177; b) T. M. Clover, C. L. O'Neill, R. Appavu, G. Lokhande, A. K. Gaharwar, A. E. Posey, M. A. White, J. S. Rudra, *J. Am. Chem. Soc.* **2020**, *142*, 19809–19813.

[15] a) A. M. Smith, R. J. Williams, C. Tang, P. Coppo, R. F. Collins, M. L. Turner, A. Saiani, R. V. Ulijn, *Adv. Mater.* **2008**, *20*, 37–41; b) R. Jain, G. Khandelwal, S. Roy, *Langmuir* **2019**, *35*, 5878–5889.

[16] a) R. Wakabayashi, A. Suehiro, M. Goto, N. Kamiya, *Chem. Commun.* **2019**, *55*, 640–643; b) R. Wakabayashi, A. Higuchi, H. Obayashi, M. Goto, N. Kamiya, *Int. J. Mol. Sci.* **2021**, *22*, 3459.

[17] M. Thomas, V. Lewe, J. Kölsch, M. Urschbach, J. Erlenbusch, O. S. Stach, P. Besenius, *Polym. Chem.* **2023**, *14*, 1888–1892.

[18] a) G. Meisl, X. Yang, E. Hellstrand, B. Frohm, J. B. Kirkegaard, S. I. A. Cohen, C. M. Dobson, S. Linse, T. P. J. Knowles, *Proc. Natl. Acad. Sci. U. S. A.* **2014**, *111*, 9384–9389; b) G. Meisl, X. Yang, C. M. Dobson, S. Linse, T. P. J. Knowles, *Chem. Sci.* **2017**, *8*, 4352–4362.

[19] E. T. Powers, D. L. Powers, *Biophys. J.* **2008**, *94*, 379–391.

[20] a) X. Wang, G. Guerin, H. Wang, Y. Wang, I. Manners, M. A. Winnik, *Science* **2007**, *317*, 644–647; b) B. B. Holmes, J. L. Furman, T. E. Mahan, T. R. Yamasaki, H. Mirbaha, W. C. Eades, L. Belaygorod, N. J. Cairns, D. M. Holtzman, M. I. Diamond, *Proc. Natl. Acad. Sci. U. S. A.* **2014**, *111*, E4376–E4385; c) S. Ogi, V. Stepanenko, K. Sugiyasu, M. Takeuchi, F. Würthner, *J. Am. Chem. Soc.* **2015**, *137*, 3300–3307; d) A. Aliprandi, M. Mauro, L. Cola, *Nat. Chem.* **2016**, *8*, 10–15; e) S. Ogi, V. Stepanenko, J. Thein, F. Würthner, *J. Am. Chem. Soc.* **2016**, *138*, 670–678; f) S. Ogi, K. Matsumoto, S. Yamaguchi, *Angew. Chem. Int. Ed.* **2018**, *57*, 2339–2343; g) G. Ghosh, S. Ghosh, *Chem. Commun.* **2018**, *54*, 5720–5723; h) E. E. Greciano, B. Matarranz, L. Sánchez, *Angew. Chem. Int. Ed.* **2018**, *57*, 4697–4701; i) X. Hao, J. Zheng, Y. Sun, X. Dong, *Langmuir* **2019**, *35*, 2821–2831; j) W. Wagner, M. Wehner, V. Stepanenko, F. Würthner, *J. Am. Chem. Soc.* **2019**, *141*, 12044–12054; k) S. Sarkar, A. Sarkar, A. Som, S. S. Agasti, S. J. George, *J. Am. Chem. Soc.* **2021**, *143*, 11777–11787; l) J. Tian, S. H. Xie, U. Borucu, S. Lei, Y. Zhang, I. Manners, *Nat. Mater.* **2023**, *22*, 786–792; m) L. Concha-Marambio, S. Pritzkow, M. Shahnawaz, C. M. Farris, C. Soto, *Nat. Protoc.* **2023**, *18*, 1179–1196; n) S. Kotha, R. Sahu, A. C. Yadav, P. Sharma, B. V. V. S. P. Kumar, S. K. Reddy, K. V. Rao, *Nat. Commun.* **2024**, *15*, 3672.

[21] J. M. Godbe, R. Freeman, J. A. Lewis, I. R. Sasselli, M. H. Sangji, S. I. Stupp, *Acta Biomater.* **2021**, *135*, 87–99.

Manuscript received: November 16, 2024
Accepted manuscript online: December 17, 2024
Version of record online: January 5, 2025